Electron dynamics at a positive ion

Bernard Talin and Annette Calisti
UMR6633, Université de Provence, Centre Saint Jérôme, 13397 Marseille Cedex 20, France

James W. Dufty
Department of Physics, University of Florida, Gainesville, Florida 32611, USA

Ilya V. Pogorelov
Accelerator and Fusion Research Division, MS 71J, Lawrence Berkeley National Laboratory, Berkeley, California 94720, USA
(Received 18 December 2007; published 27 March 2008)

The dynamics of electrons in the presence of a positive ion is considered for conditions of weak electron-electron coupling but strong electron-ion coupling. The equilibrium electron density and the electric field time correlation functions are evaluated for semiclassical conditions using a classical statistical mechanics with a regularized electron-ion interaction for molecular dynamics simulation (MD). Results are reported for the autocorrelation function of the electron electric field at the ion for $0 \leq Z \leq 40$, including conditions of strong electron-ion coupling. The electron stopping power and self-diffusion coefficient are determined from these results. Interpretation is provided by a theoretical analysis using the nonlinear Vlasov equation for the equilibrium structure, and a corresponding linear Vlasov equation for time correlation functions. The agreement of a simple mean field model with the semiclassical MD simulation is found to be quite good except for one state condition.

DOI: 10.1103/PhysRevE.77.036410 PACS number(s): 52.65.Yy, 52.25.Vy, 05.10.−a

I. INTRODUCTION

The total electric field at a particle in a plasma determines the dominant radiative and transport properties of that particle. The theory for the equilibrium distribution of fields at a neutral or charged point is well developed [1]. The theory for the dynamics of such fields is more complicated [2,3] and some progress has been made recently in special cases. For example, the field dynamics at a neutral point has been described exactly in the Holtsmark limit [4] and in linear response. The dynamical properties of fields due to *positive* ions near a positive impurity have been given an accurate approximate evaluation for a wide range of charge coupling, relative charge numbers, and relative masses [5,6]. The corresponding study of *negative* charges (electrons) at a positive ion has been considered more recently only for the simplest case of a single ion of charge number Z in a semiclassical electron gas [7–9]. In this case, the attractive interaction between the electrons and ions emphasizes further the nonlinear dependence on Z. The static properties (electron charge density, electron microfield distribution) have been discussed in some detail for this case elsewhere [7]. Time independent microfield distributions for a two component electron-ion plasma have been considered recently as well [10]. Here, attention is focused on the dynamics via the equilibrium electron electric field autocorrelation function. This case of electron fields at a positive ion is qualitatively different from same sign ion fields, since in the former case electrons are attracted to the ion leading to strong electron-ion coupling for the enhanced close configurations. A preliminary report of this work has been given in Ref. [9], and is extended here to additional state conditions (both weaker and stronger coupling conditions), a theoretical description, and further discussion of observed results.

It is difficult *a priori* to predict even the qualitative features of the field autocorrelation functions due to the inherent strong electron-ion coupling, and there is no phenomenology for guidance. Consequently, initial analysis here has been based on MD simulation of the correlation functions followed by an attempt to model and interpret the observed results. However, MD simulation for the electrons is limited to classical mechanics, while the singular attractive electron-ion interaction inherently requires a quantum mechanical description. This difficulty is circumvented by modifying the electron-ion Coulomb potential at short distances to represent quantum diffraction effects. The conditions for validity and limitations of this classical model have been discussed extensively elsewhere [11]. The details of the MD method also have been described elsewhere [7] and will not be repeated here. There is a growing recent literature on the related MD studies of two-component classical models of a hydrogen plasma [10,12,13] at stronger electron-electron coupling values, but restricted to $Z=1$. Thus the main new feature studied here is the dependence of structure and dynamics on charge number Z.

The most important dimensionless parameters are the electron-electron coupling constant $\Gamma = e^2/r_0 k_B T$, and the ion-electron coupling constant $\sigma = Z\Gamma/\delta$. The former is the average potential energy for a pair of electrons at the average separation $(4\pi n_e r_0^3/3 = 1)$ relative to the kinetic energy. The latter coupling constant is the potential energy of an electron at the ion of charge number Z relative to its kinetic energy. This depends on the quantum regularization length δ, taken here to be the de Broglie wavelength relative to the average electron separation, $\delta = (2\pi\hbar^2/m_e k_B T r_0^2)^{1/2}$. The electron coupling considered is $\Gamma \leq 0.5$, so electron-electron interactions can be considered as weak (but not negligible). In contrast, strong electron-ion coupling is included with $0.5 \leq \sigma \leq 10$.

The potentials and state conditions are defined further in the next section and the MD simulation of the electric field due to all electrons at the ion is described briefly. In particular, the occurrence of close, orbiting trajectories is noted for larger values of σ. The primary derived property to characterize the dynamics is the autocorrelation function of this field. The primary observations from this function for increasing electron-ion coupling are: (1) an increase in the initial value (the field covariance), (2) a decrease in the correlation time, and (3) the appearance of an increasing anticorrelation at intermediate times. It is noted that several physical properties are determined from the time integral of the autocorrelation function (e.g., stopping power, friction and diffusion coefficients, spectral line widths). The integrals obtained from the MD simulation data show a decrease in value as a function of σ, indicating that the dynamical effects (2) and (3) above dominate the static correlation effect (1).

To interpret these results, particularly the dynamical effects, a kinetic theory is considered. Since Γ is small the kinetic equation for the electron reduced distribution function becomes the nonlinear Vlasov equation in the presence of the external ion potential. For the equilibrium state (electron excess density around the ion) this equation gives the nonlinear Boltzmann-Poisson equation, whose solution is in good agreement with the MD simulation results [7].

The field autocorrelation function is determined from the linearized Vlasov equation (linear perturbations of the equilibrium state, but still nonlinear in the electron-ion interaction). The results are a composition of correlated initial conditions, single electron trajectories in an effective potential about the ion, and dynamical collective screening by the inhomogeneous electron distribution about the ion. It is assumed that the most important features are the initial correlations and mean field single particle trajectories leading to a practical approximation. This theoretical analysis of the electric field autocorrelation function shows reasonable agreement with the results from MD simulation. In particular, the simple mean field approximation reproduces all of the above qualitative features (1)–(3). Furthermore, its simplicity allows a physical interpretation of those results consistent with observations from MD simulation.

In the low velocity limit, and for large ion mass, the stopping power is proportional to the time integral of the field autocorrelation function [14,15]. Linear response predicts a dominant Z^2 dependence for these properties. Significant deviations from this Z^2 dependence are observed at strong coupling and have been the focus of attention in recent years [16]. The results here show these deviations come from a competition between the increase of the integral due to (1) above and the decrease due to (2) and (3). MD simulation shows that the latter two dynamical effects dominate the former static effect. The simple mean field model provides the missing interpretation for (2) and (3).

This same integral of the field autocorrelation function determines the half width for spectral lines from ion radiators due to perturbations by electrons in the fast fluctuation limit [17]. An application of MD simulation similar to this atomic physics problem has been carried out and promises to provide an additional experimental probe for the dynamics of charges near an ion [18,19].

The MD results are provided in the next section. The kinetic theory and mean field approximation are given in Secs. III and IV, and compared to the MD results. Application to the stopping power is presented in Sec. V. Finally, a discussion and summary are provided in the last two sections.

II. MD SIMULATION RESULTS

The classical system considered consists of N_e electrons with charge $-e$, an infinitely massive positive ion with charge Ze placed at the origin, and a rigid uniform positive background for overall charge neutrality contained in a large volume V. The Hamiltonian has the form

$$H = \sum_{\alpha=1}^{N_e} \left(\frac{p_\alpha^2}{2m} + V_{ei}(r_\alpha) + V_{eb}(r_\alpha) \right) + \frac{1}{2} \sum_{\alpha,\gamma}^{N_e} V_{ee}(|\mathbf{r}_\alpha - \mathbf{r}_\gamma|), \tag{1}$$

where $V_{ee}(|\mathbf{r}_\alpha - \mathbf{r}_\gamma|)$ is the Coulomb interaction for electrons α and γ, $V_{ei}(r_\alpha)$ is the regularized electron-ion interaction for electron α with the ion, and $V_{eb}(r_\alpha)$ is the Coulomb interaction for electron α with the uniform neutralizing background

$$V_{ee}(|\mathbf{r}_\alpha - \mathbf{r}_\gamma|) = \frac{e^2}{|\mathbf{r}_\alpha - \mathbf{r}_\gamma|}, \quad V_{ei}(r_\alpha) = -Ze^2 \frac{(1 - e^{-r_\alpha/r_0\delta})}{r_\alpha}, \tag{2}$$

$$V_{eb}(r_\alpha) = -\left(1 - \frac{Z}{N_e}\right) n_e \int d\mathbf{r} V_{ee}(|\mathbf{r}_\alpha - \mathbf{r}|). \tag{3}$$

Note that due to symmetry of the cubic cells, the neutralizing background does not affect particle motion in MD simulations. For values of $r/r_0 \gg \delta$ the potential $V_{ei}(r)$ becomes Coulomb, while for $r \ll \delta$ the Coulomb singularity is removed and $\beta V_{ei}(r) \to -\beta Ze^2/r_0\delta = -Z\Gamma/\delta = -\sigma$. This is the simplest phenomenological form representing the short range effects of the uncertainty principle [20]. In principle, there should be a similar regularization of the electron-electron interaction, but since that interaction is repulsive, configurations with a pair of electrons within a thermal de Broglie wavelength are rare. For simplicity, therefore, the electron-electron interaction is taken to be Coulomb. In all of the following the electron-electron coupling (weak) is measured by Γ while that for the electron-ion coupling (possibly strong) is measured by σ. The three state conditions considered are shown in the following table:

n (cm^{-3})	T (K)	Γ	σ	δ
1×10^{19}	2×10^5	0.029	$0.5Z$	0.058
2.5×10^{22}	7.9×10^5	0.1	$0.25Z$	0.4
3.2×10^{18}	7.9×10^3	0.5	$2.5Z$	0.2

A. Electron density

The most important structural property for this system is the nonuniform electron distribution about the impurity ion. It can be expressed in terms of a Boltzmann factor with an effective electron-ion potential

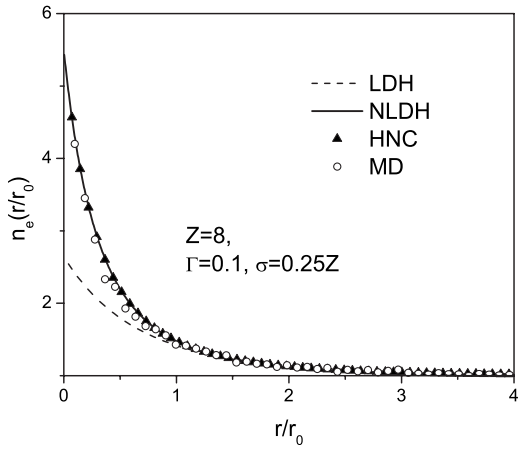

FIG. 1. Electron density excess around an ion of charge number $Z=8$.

$$n_e(r) \equiv n_e e^{-\beta U_{ei}(r)}. \tag{4}$$

For the conditions of weak electron-electron coupling $U_{ei}(r)$ obeys the nonlinear integral equation

$$U_{ei}(r) = V_{ie}(r) + n_e e^2 \int d\mathbf{r}' \frac{1}{|\mathbf{r}-\mathbf{r}'|}(e^{-\beta U_{ei}(r')} - 1). \tag{5}$$

This is an integral form of the Boltzmann-Poisson equation for the regularized electron-ion potential (see the kinetic theory section below). The second term provides the nonlinear strong coupling effects of the electron-ion interactions. It is worth noting that although the electron-electron coupling is weak, the strong ion-electron effects are mediated by the electron-electron interaction of this second term. The predictions for a free electron gas interacting with an ion are quite different from those given below.

The numerical solutions to Eq. (5) and its relationship to the hypernetted chain (HNC) integral equation [21] at stronger electron coupling have been discussed in Ref. [7]. At the weak electron-electron coupling considered here these equations are the same as the HNC equations, and their solution in the following will be referred to as the HNC result. An important observation in Ref. [7] is that the numerical solution is well represented by the Debye form

$$U_{ei}(r') = \frac{-\bar{Z}e^2}{(1-(\delta/\bar{\lambda})^2)}\frac{1}{r}(e^{-r/r_0\bar{\lambda}} - e^{-r/r_0\delta}), \tag{6}$$

where the effective charge number $\bar{Z}$ and screening length $\bar{\lambda}$ are fitting parameters. In the weak coupling domain these become the actual charge number and the Debye screening length and this form is exact. More generally, it is only an approximation and the best choices for $\bar{Z},\bar{\lambda}$ are different from Z, λ at strong coupling. This approximation for $n_e(r)$ will be referred to as the nonlinear Debye-Huckel (NLDH) approximation. Figure 1 illustrates the results from MD simulation and their fitting by the nonlinear Debye form and the solution to Eq. (5) for the case $Z=8$, $\Gamma=0.1$, and $\delta=0.4$. The agreement is quite good, providing a simple, physical interpretation of the MD results. Finally, the linear Debye-Huckel (LDH) form is shown to indicate that nonlinear effects are clearly significant. Similar results are obtained for the other values of Z discussed below. A more complete discussion of the structural results from MD is given in Ref. [7].

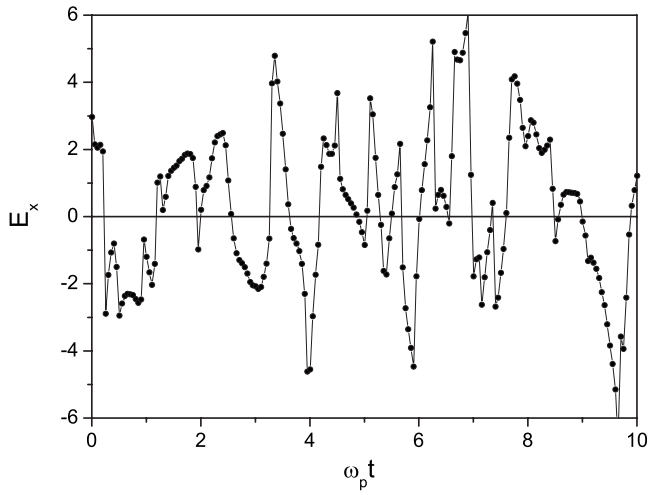

FIG. 2. x component of the electric field for $\sigma=5$.

B. Electric field dynamics

The application of standard MD simulation methods using the semiclassical electron-ion potential is somewhat more complex than for the usual classical fluids with short range repulsive interactions. Although finite at short distances the attractive electron-ion potential allows bound and metastable states for electrons orbiting around the ion over extended periods. For most properties, e.g., the electron density above, this is not a severe problem except at low temperatures. However, the interest here is in electric field dynamics, which is very sensitive to close electron-ion configurations.

The total electric field at the impurity ion due to all electrons is given by

$$\mathbf{E} = \frac{1}{Ze}\sum_{\alpha=1}^{N_e} \boldsymbol{\nabla}_{r_\alpha} V_{ei}(r_\alpha) = \sum_{\alpha=1}^{N_e} \mathbf{e}(\mathbf{r}_\alpha), \tag{7}$$

$$\mathbf{e}(\mathbf{r}_\alpha) = e\frac{\hat{\mathbf{r}}_\alpha}{r_\alpha^2}\left[1 - \left(1 + \frac{r_\alpha}{r_0\delta}\right)e^{-r_\alpha/r_0\delta}\right]. \tag{8}$$

Figure 2 shows an example of one component of the electric field for $Z=20$, $\Gamma=0.1$, and $\delta=0.4$, corresponding to the strong coupling condition of $\sigma=5$. For such conditions the electric field develops strong oscillations that are rather coherent over times large compared to the characteristic inverse plasma frequency. Evidently, this is due to a few electrons executing quasibound trajectories due to the strong attraction of the impurity, as illustrated in Fig. 3. On a still longer time scale, these oscillating fields break up and new ones appear. The MD simulations must be performed on a time scale long enough to sample the entire ensemble of such oscillatory configurations. At very strong coupling (beyond the range

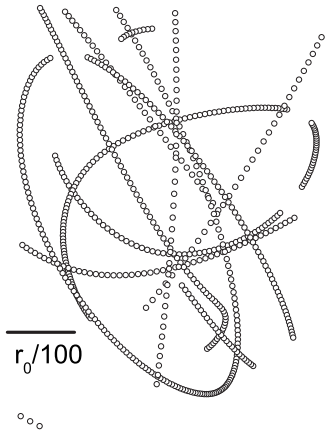

FIG. 3. Example of a single electron trajectory around the ion; same conditions as Fig. 2.

considered here), the oscillations persist on very long time scales, prohibiting a proper statistical analysis of the simulation data. The protocol for control of such anomalous states with quasibound dynamical states has been described in Ref. [7] and will not be repeated here.

To explore the dynamics of the electrons in more detail attention is limited to the electric field autocorrelation function defined by

$$C(t) = \frac{r_0^4}{e^2}\langle \mathbf{E}(t) \cdot \mathbf{E} \rangle. \tag{9}$$

The brackets denote an equilibrium Gibbs ensemble average. Consider first the initial value $C(0)$. It is shown in Appendix A that it can be determined from the effective potential in Eq. (5) according to

$$C(0) = \frac{r_0^4}{e^2} \int d\mathbf{r} n_e(r) \mathbf{e}_{mf}(\mathbf{r}) \cdot \mathbf{e}(\mathbf{r}), \tag{10}$$

$$\mathbf{e}_{mf}(\mathbf{r}) = -\frac{1}{\beta Z e} \nabla \ln n_e(r).$$

Figure 4 shows the initial field fluctuations $C(0)$ as a function of Z, at $\Gamma=0.1$, $\sigma=0.25Z$, and at $\Gamma=0.5$, $\sigma=2.5Z$ calculated using $n_e(r)$ from Eqs. (4) and (5) in comparison with the results from MD simulation. The agreement is quite good, both showing a strong Z dependence due to the increasing electron charge density near the impurity for larger Z. The results for the third coupling condition, $\sigma=0.5Z$, are discussed in the final section.

The dynamics of the field autocorrelation function is shown for $\Gamma=0.1$, $\sigma=0.25Z$ in Fig. 5. The electron-ion coupling ranges from $\sigma=1$ to $\sigma=10$. There are two qualitative features to note. The first is a characteristic time for relaxation that decreases with increasing coupling, and the second is the development of an anticorrelation that increases with increasing coupling. Figures 6 and 7 show the corresponding results for the other two cases ($\sigma=2.5Z$, $Z=1,2,3,4,6,10$) and $\sigma=0.5Z$, $Z=1,3,5,8$. The strongest coupling case of Fig. 6 shows large anticorrelation for all Z. It should be noted

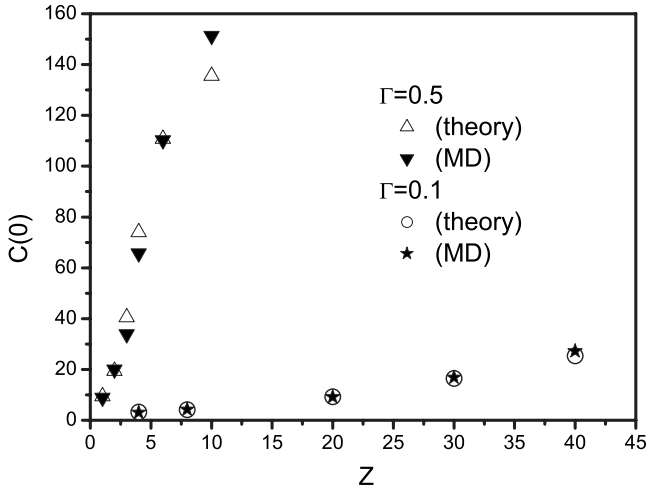

FIG. 4. Initial value for the electric field autocorrelation function.

that this last case is somewhat unrealistic since the equilibrium population of ions at such strong coupling is extremely small. In the weaker coupling cases of Fig. 7 the decreasing relaxation time is evident but the anticorrelation is significant only for the $Z=8$ curve.

The area under the curves is related to transport properties, as indicated below, and results from a competition between these two features and the increasing initial correlations. The effects of shortening decay time and anticorrelation dominate to decrease the area as indicated in Fig. 8. These effects are greater for stronger coupling, with significant anticorrelation occurring for $Z \geq 4$.

III. KINETIC THEORY

To interpret the qualitative features of $C(t)$ identified in the above simulations and to identify their underlying mechanisms, it is useful to have a corresponding theoretical

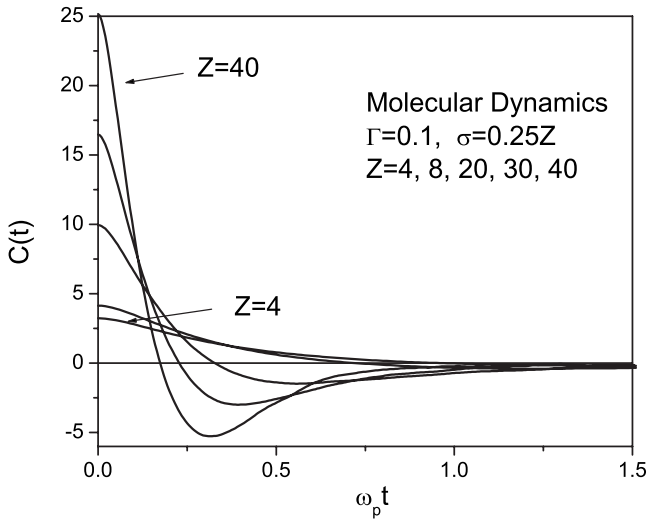

FIG. 5. Field autocorrelation function at $\sigma=0.25Z$.

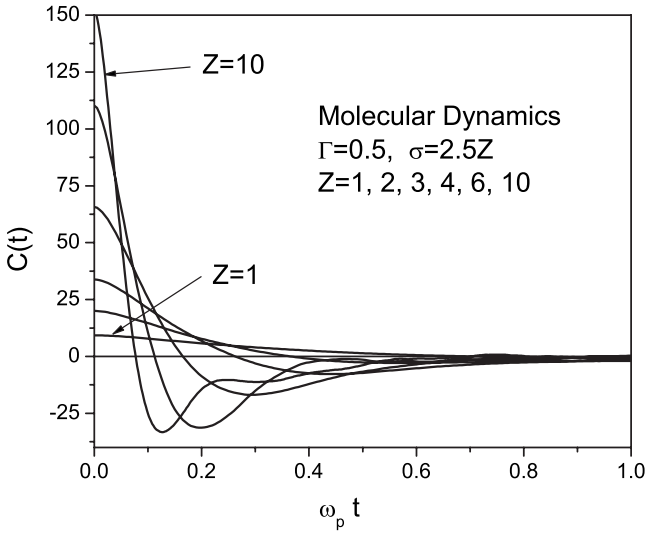

FIG. 6. Field autocorrelation function at $\sigma=2.5Z$.

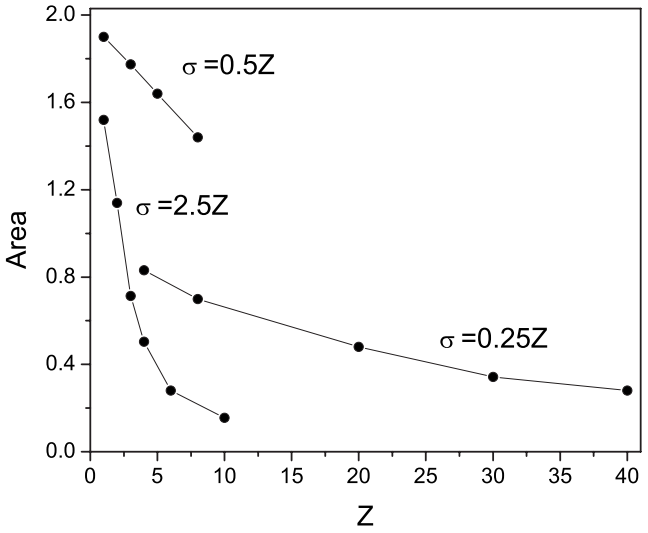

FIG. 8. Time integral of $C(t)$ as a function of Z.

model. This is provided by kinetic theory for weakly coupled electrons in the presence of an ion. The distribution function for the electrons is denoted by $f(\mathbf{r},\mathbf{v};t)$. It is normalized such that integration over all velocities and the volume of the system equals N_e, and obeys the exact first BBGKY (Born, Bogoliubov, Green, Kirkwood, Yvon) hierarchy equation [22],

$$(\partial_t + \mathbf{v}\cdot\boldsymbol{\nabla}_{\mathbf{r}} - m_e^{-1}\{\boldsymbol{\nabla}_{\mathbf{r}}[V_{ei}(\mathbf{r}) + V_{eb}(\mathbf{r})]\}\cdot\boldsymbol{\nabla}_{\mathbf{v}})f(\mathbf{r},\mathbf{v};t) = m_e^{-1}\int d\mathbf{r}_2 d\mathbf{v}_2[\boldsymbol{\nabla}_{\mathbf{r}}V_{ee}(\mathbf{r}-\mathbf{r}_2)]\cdot\boldsymbol{\nabla}_{\mathbf{v}}f^{(2)}(\mathbf{r},\mathbf{v};\mathbf{r}_2,\mathbf{v}_2;t). \tag{11}$$

Here $f^{(2)}(\mathbf{r},\mathbf{v};\mathbf{r}_2,\mathbf{v}_2;t)$ is the joint distribution function for two electrons. At weak coupling ($\Gamma \ll 1$) the electron distributions are approximately independent and $f^{(2)}(\mathbf{r},\mathbf{v};\mathbf{r}_2,\mathbf{v}_2;t)\to f(\mathbf{r},\mathbf{v};t)f(\mathbf{r}_2,\mathbf{v}_2;t)$. Then Eq. (11) becomes the nonlinear Vlasov equation,

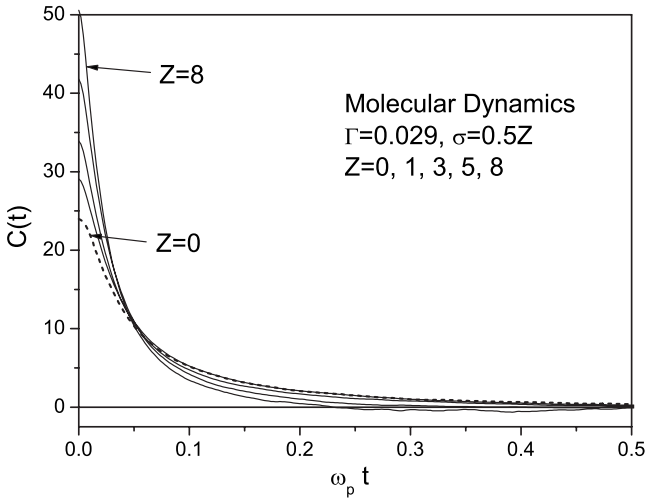

FIG. 7. Field autocorrelation function at $\sigma=0.5Z$.

$$(\partial_t + \mathbf{v}\cdot\boldsymbol{\nabla}_{\mathbf{r}} - m_e^{-1}\{\boldsymbol{\nabla}_{\mathbf{r}}[V_{ei}(\mathbf{r})]\}\cdot\boldsymbol{\nabla}_{\mathbf{v}})f(\mathbf{r},\mathbf{v};t) = m_e^{-1}[\boldsymbol{\nabla}_{\mathbf{v}}f(\mathbf{r},\mathbf{v};t)]\cdot\boldsymbol{\nabla}_{\mathbf{r}}\int d\mathbf{r}_2 V_{ee}(\mathbf{r}-\mathbf{r}_2)\delta n(\mathbf{r}_2,t), \tag{12}$$

where $\delta n(\mathbf{r},t)$ is the deviation of the electron density from the rigid uniform positive background

$$\delta n(\mathbf{r},t) = n(\mathbf{r},t) - \left(1-\frac{Z}{N_e}\right)n_e, \quad n(\mathbf{r},t) = \int d\mathbf{v} f(\mathbf{r},\mathbf{v};t). \tag{13}$$

Note that this approximation does not imply weak electron-ion coupling and so it is applicable for the range of Z considered in the simulations. The stationary solution is given by a Maxwellian velocity distribution times the density $n_e(r)$ in Eqs. (4) and (5).

The left side of Eq. (12) describes the single electron motion in the presence of the ion at the origin. Since the charge number can be large, the electron ion coupling can be large. The right side of this equation describes the correlation effects due to interactions among the electrons, which are weak for hot, dense matter. However, these weak correlations depend nonlinearly on the distribution function so that the content of this equation and its solutions can be quite rich and complex.

It is shown in Appendix B that the time dependence of $C(t)$ in the weak coupling limit can be written as

$$C(t) = \int d\mathbf{r} d\mathbf{v} \mathbf{e}(\mathbf{r})\cdot\psi(\mathbf{r},\mathbf{v},t), \tag{14}$$

where $\psi(\mathbf{r},\mathbf{v},t)$ obeys the linear Vlasov equation

$$(\partial_t + \mathcal{L})\psi(\mathbf{r},\mathbf{v};t) = -\beta f_e(\mathbf{r},\mathbf{v})\mathbf{v}\cdot\boldsymbol{\nabla}_\mathbf{r}\int d\mathbf{r}_2 V_{ee}(\mathbf{r}-\mathbf{r}_2) \times \int d\mathbf{v}_2 \psi(\mathbf{r}_2,\mathbf{v}_2,t). \quad (15)$$

The associated initial condition is

$$\psi(\mathbf{r},\mathbf{v},t=0) = \mathbf{e}_{mf}(\mathbf{r})f_e(\mathbf{r},\mathbf{v}), \quad \mathbf{e}_{mf}(\mathbf{r}) = \frac{1}{Ze}\nabla U_{ei}(\mathbf{r}), \quad (16)$$

where $U_{ei}(\mathbf{r})$ is the effective potential associated with the number density in Eq. (4) above. The linear operator $\mathcal{L}$ is the generator for single electron dynamics in this effective potential $U_{ei}(\mathbf{r})$,

$$\mathcal{L} = \mathbf{v}\cdot\boldsymbol{\nabla}_\mathbf{r} - m_e^{-1}\{\boldsymbol{\nabla}_\mathbf{r}[U_{ei}(\mathbf{r})]\}\cdot\boldsymbol{\nabla}_\mathbf{v}. \quad (17)$$

The equilibrium distribution is stationary under this operator, $\mathcal{L}f_e(\mathbf{r},\mathbf{v})=0$. In addition to this effective single particle dynamics, all dynamical many-electron effects are contained in the term on the right side of Eq. (15). The details of the formal solution to this kinetic equation for the correlation function are given in Appendix C with the result

$$C(t) = \int_0^t dt' \int d\mathbf{r}d\mathbf{v} f_e(\mathbf{r},\mathbf{v})\mathbf{e}_s(\mathbf{r};t')\mathbf{e}_{mf}[\mathbf{r}(t-t')]. \quad (18)$$

The field $\mathbf{e}[\mathbf{r}(t-t')]$ is given by Eq. (8) with the initial position shifted to $\mathbf{r}(t-t')$ according to the effective single particle dynamics generated by $\mathcal{L}$, using the initial conditions $\mathbf{r},\mathbf{v}$. The other field $\mathbf{e}_s(\mathbf{r};t')$ is a dynamically screened field

$$\mathbf{e}_s(\mathbf{r};t) = (2\pi)^{-3}\int d\mathbf{k} e^{-i\mathbf{k}\cdot\mathbf{r}}\tilde{\mathbf{e}}_s(\mathbf{k},t), \quad (19)$$

$$\tilde{\mathbf{e}}_s(\mathbf{k},t) = \int d\mathbf{k}'\tilde{\mathbf{e}}(\mathbf{k}')\epsilon^{-1}(\mathbf{k}',\mathbf{k},t),$$

where $\tilde{\mathbf{e}}(\mathbf{k}')$ is the Fourier transform of Eq. (8), and the dielectric function is defined by

$$\epsilon(\mathbf{k},\mathbf{k}',t) = (2\pi)^3\delta(\mathbf{k}-\mathbf{k}') + \pi(\mathbf{k},\mathbf{k}',t)\tilde{V}_{ee}(k'), \quad (20)$$

$$\pi(\mathbf{k},\mathbf{k}',t) = \beta\frac{d}{dt}\int d\mathbf{r}d\mathbf{v} f_e(\mathbf{r},\mathbf{v})e^{i\mathbf{k}\cdot\mathbf{r}}e^{-i\mathbf{k}'\cdot\mathbf{r}(t)}. \quad (21)$$

For $Z=0$ this is the familiar classical random phase approximation for a uniform electron gas, diagonal in $\mathbf{k},\mathbf{k}'$. More generally, the Z dependence leads to a nonuniform electron density near the ion and the polarization function $\pi(\mathbf{k},\mathbf{k}',t)$ depends on the details of this distribution. It vanishes at $t=0$ indicating no initial screening, $\pi(\mathbf{k},\mathbf{k}',t=0)=0$. At later times the polarization function is nonzero giving a space and time dependent additional screening. Further simplification of this result for practical evaluation is discussed below.

IV. EFFECTIVE SINGLE PARTICLE MODEL

To calculate the correlation function and identify the mechanisms for the decay time and correlation, it might be supposed that the single nearest electron dominates since its field is greatest. Figure 9 shows this nearest neighbor contribution from MD for the same conditions of Fig. 5. Clearly, the nearest neighbor field autocorrelation function has the same qualitative Z dependence as the total correlation function with respect to the decreasing decay time and increasing anticorrelation. The quantitative values are wrong (both amplitude and time scale), however, suggesting that contributions from other electrons are important as well. To explore this in more detail, the result from the Vlasov equation given by Eq. (18) can be used. It requires evaluation of the dynamically screened field $\mathbf{e}_s(\mathbf{r};t)$, although the screening at short times vanishes. The correlation function is then effectively that for a single particle moving in the self-consistent potential (5), averaged over the initial equilibrium distribution of electrons about the ion. Thus it is similar to the nearest neighbor approximation but extends it to include all electrons, providing the correct initial correlations and the correlations of the mean field for the dynamics. If the additional *dynamical* screening is neglected for all relevant times, i.e.,

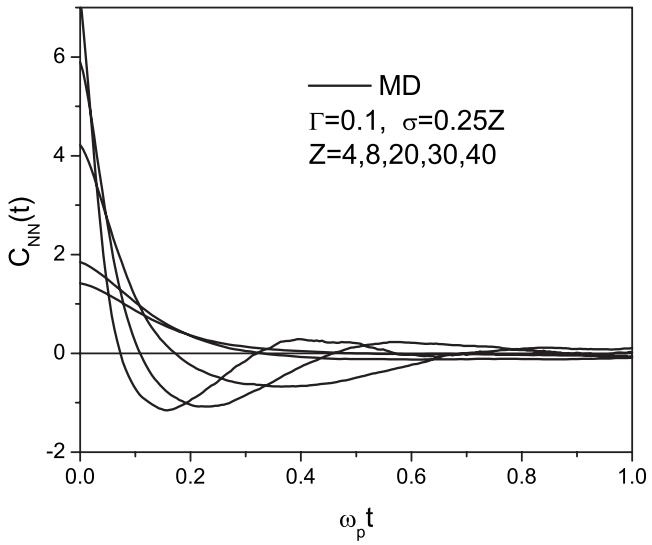

FIG. 9. Nearest neighbor field autocorrelation function for strong coupling.

$$\mathbf{e}_s(\mathbf{r};t) \to \delta(t)\mathbf{e}(\mathbf{r}), \quad (22)$$

then Eq. (18) becomes

$$C(t) \to \int d\mathbf{r}d\mathbf{v} f_e(\mathbf{r},\mathbf{v})\mathbf{e}(\mathbf{r})\mathbf{e}_{mf}[\mathbf{r}(t)]. \quad (23)$$

Comparison with Eq. (10) shows that this approximation is exact for $C(0)$. For practical purposes, this approximation for $C(t)$ has been evaluated using the analytic nonlinear Debye form (6) fitted to the HNC results for the electron density. The dynamics for this effective single particle model are shown in Figs. 10 and 11 for $C(t)/C(0)$ at $\Gamma=0.1$ and $\sigma=0.25Z$.

The agreement of this simple theory with MD simulation is quite reasonable and provides a means to interpret the simulation results (some of the differences are due to the

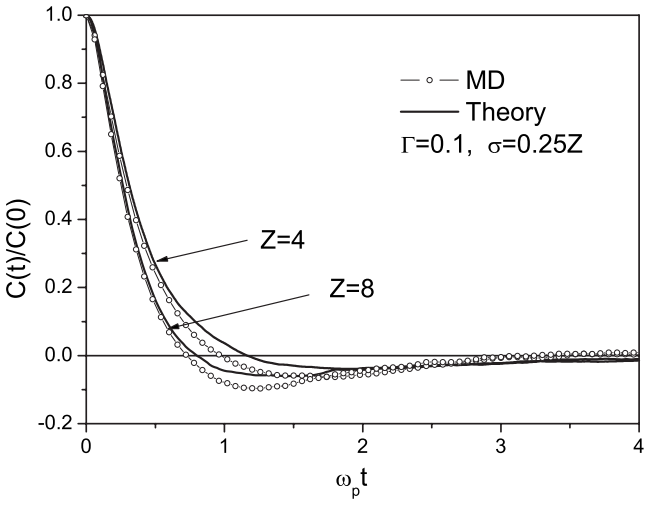

FIG. 10. Comparison of $C(t)$ from MD with results from mean field kinetic theory for $Z=4,8$.

subjective fitting of the nonlinear Debye form). The initial position and velocity of an electron are sampled from the equilibrium distribution $f_e(\mathbf{r},\mathbf{v})$ which favors electrons close to the ion and hence large fields. Since the force on the electron is also large, its initial acceleration will be large. This is the source of the short decay time. Consider the case of an energetic electron near the ion. If its velocity is directed away from the ion it will move to larger distances and the field will decrease with a positive component along the initial field. In contrast, if its initial velocity is toward the ion it will move past the ion with a change in the direction of its field relative to the initial value. This is a source for anticorrelation. For less energetic electrons, the trajectories are bound and there is continual correlation and anticorrelation as the correlation function decays in magnitude due to phase averaging. Both the increase in initial correlation and the field reversal effects should increase as the charge on the ion increases, and this is what is observed. At weaker electron-ion coupling both effects are diminished and blurred as the relevant configurations are more distant, the fields are weaker, and the accelerations smaller. This is already evident in the nearest neighbor results of Fig. 9.

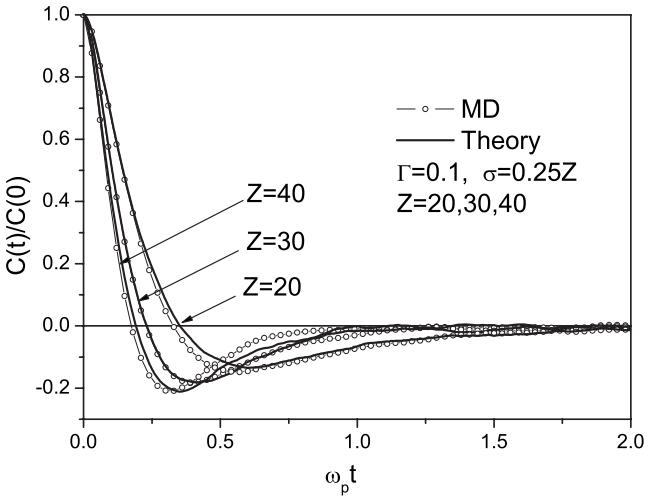

FIG. 11. Same as Fig. 10 for $Z=20,30,40$.

The simple model of Eq. (23) appears better at larger values of Z where the single particle motion is expected to dominate. For smaller values of Z the agreement at short times is still good, but more significant differences occur after the first initial decrease. Presumably, this is due to the dynamical screening effects in $\mathbf{e}_s(\mathbf{r};t)$ that have been neglected. As noted above, the results are also somewhat sensitive to the choice of parameters $\bar{Z},\bar{\lambda}$ used in fitting the nonlinear Debye-Huckel form for $f_e(\mathbf{r},\mathbf{v})$. Fits emphasizing short or intermediate distances change slightly the point at which anticorrelation sets in and its amplitude. The primary criterion used here was a globally good visual fit and a good resulting value for the initial condition $C(0)$.

V. STOPPING POWER, FRICTION, AND SELF-DIFFUSION

Emphasis here has been placed on the electric field autocorrelation function as a sensitive measure of electron properties near the ion. This function is also of interest because of its connection to transport and radiative properties of the ion. Specifically, for the case of an infinitely massive ion considered here there are exact relationships between transport coefficients characterizing three physically different phenomena: (1) the low velocity stopping power $\mathcal{S}$ for a particle injected in the electron gas, (2) the friction coefficient ξ for the resistance to a particle being pulled through the gas, and (3) the self-diffusion coefficient D of a particle at equilibrium with the gas [15],

$$m_0\xi = (\beta D)^{-1} = \left.\frac{\mathcal{S}(v)}{v}\right|_{v=0} = \beta Z^2 r_0^{-4}\int_0^\infty dt C(t). \quad (24)$$

Finally, the time integral of $C(t)$ also provides the fast fluctuation limit (impact) for the spectral linewidth of ionic radiators broadened by electrons [23]. Clearly, a better understanding of the mechanisms controlling the electric field autocorrelation function is of interest in several different contexts.

This Green-Kubo representation (24) allows a determination of these transport properties from an equilibrium MD simulation, as described above. In contrast, previous simulations of stopping power have studied the nonequilibrium state of the injected particle, measuring directly the energy degradation [16]. At asymptotically weak coupling, these properties have a dominant Z^2 dependence, as $C(t)$ becomes independent of Z. An interesting result of the previous simulations [16], and some experiments [24], was the observation of a weaker Z dependence at strong coupling. This behavior is somewhat puzzling in light of the strong growth of the initial value $C(0)$ at large Z (see Fig. 4), suggesting an enhanced dependence on Z. However, as Fig. 8 shows clearly the competing effects of decreasing correlation time and a developing time interval of anticorrelation dominate at strong coupling to decrease the time integral. Figure 12 shows the dimensionless stopping power as a function of Z for the case $\Gamma=0.1$ and $\sigma=0.25Z$. Also shown is the Born

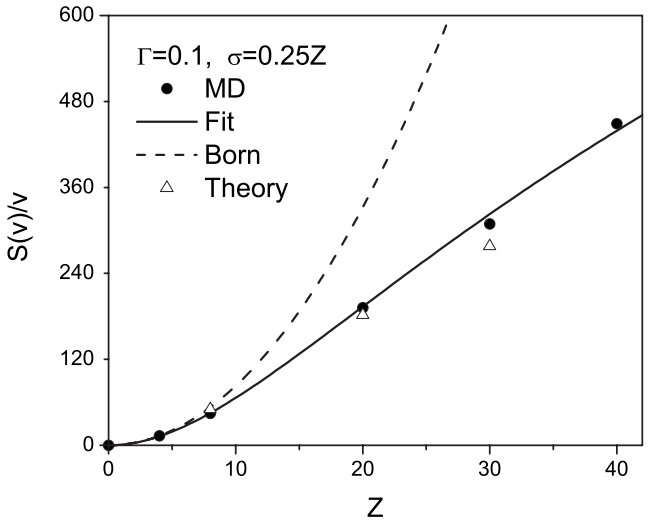

FIG. 12. Stopping power relative to the speed at zero speed, Eq. (24), at strong coupling. Also shown are the Born approximation and the results of the kinetic theory.

approximation $0.83Z^2$, where the coefficient has been determined by the data for small Z. The MD data has been fit to a crossover function

$$\left.\frac{\mathcal{S}(v)}{v}\right|_{v=0} \to \frac{0.83Z^2}{1+0.008Z^{1/2}}. \tag{25}$$

This form has been chosen since it implies the stopping power goes as $Z^{3/2}$ at extreme coupling, which is consistent with the earlier results [16,24]. However, other fits to the data here are possible as well. The predictions of the simple effective single particle theory also are shown in Fig. 12.

Similar results are obtained for the other coupling cases. Figure 13 shows the stopping power for the strongest coupling case of $\Gamma=0.5$ and $\sigma=2.5Z$. The Born approximation is determined from the $Z=1$ data and found to be $1.52Z^2$. The deviations from the Born approximation are much greater now, as expected. The weaker electron-electron coupling case of $\Gamma=0.029$ and $\sigma=0.5Z$ is shown in Fig. 14, where the Born approximation $1.88Z^2$ is again determined by the $Z=1$

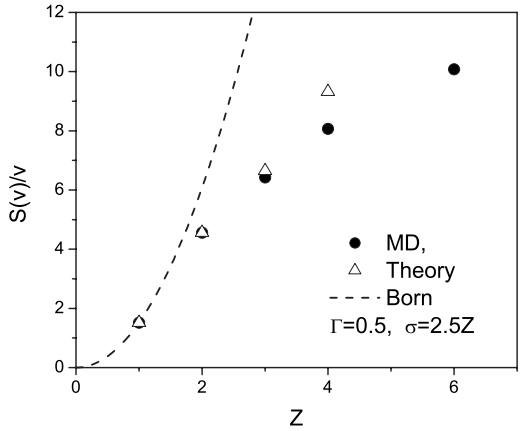

FIG. 13. Same as Fig. 12 at very strong coupling.

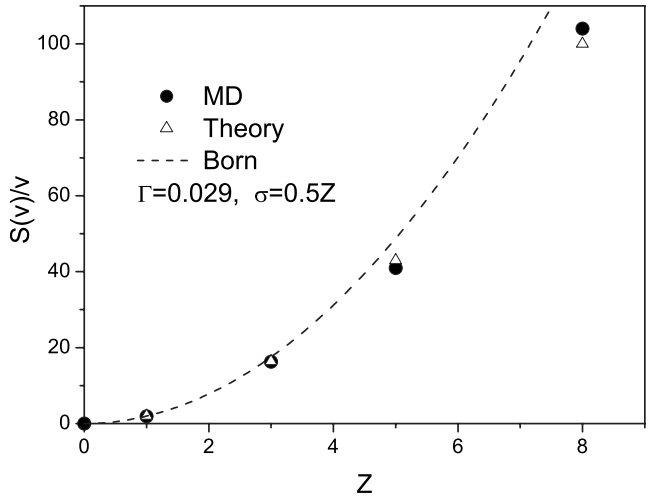

FIG. 14. Same as Fig. 12 at moderate coupling.

value. As expected the Born approximation is quite good at weak coupling, although some deviation is seen at $Z=8$. This is consistent with an estimate from all cases that strong coupling effects occur for $Z\sigma \geq 4$. It will be shown in the following section that the quite good agreement observed between theory and MD in Fig. 14 results from a balance between covariance and anticorrelation in the autocorrelation function integration.

VI. DISCUSSION

The electric field autocorrelation function is an interesting probe for electron dynamics in the presence of a positive ion since it is sensitive to the enhanced electron density near the ion. The simple theoretical model given above provides a means to interpret the MD simulation data for the beginnings of a phenomenological understanding of electron dynamics near a positive ion. The initial correlation for the electric field $C(0)$ increases with Z as the equilibrium distribution of electrons is enhanced near the ion with configurations corresponding to larger fields. The latter is well described by the nonlinear Debye-Huckel form given by Eq. (4) with Eq. (6). The initial decay of $C(t)$ is essentially the decorrelation time for a "most probable" electron near the ion. This most probable distance can be estimated from the maximum of the Debye distribution $P(r)=4\pi r^2 n_e(r)/n_e \equiv 4\pi r^2 e^{-\beta U_{ei}(r)}$ to give $r/r_0 \sim \delta$ for strong coupling. The correlation time is then approximately the time to accelerate this electron to the position of the ion, $t_c \sim (r_0\delta/\sqrt{\beta m})\sqrt{1/Z\Gamma}$. The first factor $r_0\delta/\sqrt{\beta m}$ is the time for an electron with the thermal velocity to cross a sphere of the size of the thermal de Broglie diameter. The second factor gives the dominant Z dependence $t_c \sim \sqrt{1/Z}$. As the electron continues past the ion its acceleration changes sign as it is attracted to the ion with a field opposite that of the original field. This is the source of the dominant anticorrelation.

The self-diffusion coefficient, stopping power, friction coefficient, and width of spectral lines are proportional to the integral of $C(t)$. At $Z=0$ this is the field autocorrelation func-

tion at a neutral point and is independent of Z, depending only on the electron-electron coupling. As Z increases the electron distribution becomes nonuniform about the ion and $C(0)$ increases. At the same time t_c decreases. For small Z these two effects become negligible, as seen in Fig. 7 for the case of $\sigma=0.5Z$ and $Z<5$. As Z increases, or more precisely as σ increases, the domain of anticorrelation appears and begins to dominate the decrease in the integral of $C(t)$. These basic mechanisms are captured by the mean field description based on the Vlasov equation for the one particle electron distribution. The relevant correlations contained in this description are those of the equilibrium electron distribution about the ion, also described well by the stationary solution to the Vlasov equation.

This analysis provides a new picture for the decrease of stopping power with increasing Z, relative to the Born approximation. The stopping power is proportional to Z^2 times the time integral of $C(t)$, which is essentially the total cross section for all the electrons and the ion. The decrease towards a $Z^{3/2}$ dependence at strong coupling observed earlier [16] is seen to be due to the effects just described. However, the precise dependence on Z may be more complicated as the coupling increases. The extensive discussion of Ref. [16] exposes a number of sources for the deviations from the Born approximation observed in those simulations. A detailed comparison with the results obtained there has not been made as each represents a different classical model for the real quantum system, and different states were simulated (equilibrium or nonequilibrium). While the physical effects being modeled are the same in both cases, somewhat different treatments of the short distance screening and extrapolation to linear stopping make quantitative comparisons inappropriate and without any clear means to interpret any differences. Instead, the work here focuses on identifying mechanisms behind the observed qualitative behavior for a reasonable model and indeed agreement with the earlier work in [16] is found at that level.

Similarly, these same results provide clear evidence for the effects of electron-electron and electron-ion correlations on the shape of spectral lines [18,19]. It is expected that analogous experimental puzzles regarding the Z dependence of the half width [25] could be clarified through theoretical and MD simulation as described here.

In closing this section, an unexpected and unresolved discrepancy between MD simulation and the theory is discussed. This occurs for the weakest electron-electron coupling condition of $\Gamma=0.029$. Figure 15 shows a comparison of $C(t)/C(0)$ from theory and simulation, with good agreement at $Z=1$ and no agreement at $Z=8$. The latter corresponds to a strong coupling condition of $\sigma=4$, but this value at $\Gamma=0.1$ and $\Gamma=0.5$ shows good agreement between theory and simulation. A similar strong disagreement between theory and simulation is found for $C(0)$ at $\Gamma=0.029$ as shown in Fig. 16. This identifies the source of the problem as being the electron density, since $C(0)$ is entirely determined by that density [see Eq. (10)]. Furthermore, the discrepancy appears to be due to differences for positions near the ion. This is illustrated by the distribution for electric fields shown in Fig. 17 for $\Gamma=0.029$ and $Z=8$, where the theory is seen to predict an enhancement of large fields (short distances) relative to the simulations. In most of the above discussion only the two coupling parameters Γ and σ have been emphasized, but there is an additional independent parameter δ as well. As noted above, $r/r_0 \sim \delta$ is the most probable position for an electron. The discrepancies between theory and simulation occur for the smallest value of $\delta=0.06$ considered, and therefore the case with closest approach of the electrons to the ion. However, since the electron-electron coupling is weakest as well, the theory might be thought to be most reliable. For these weak coupling conditions, Eqs. (4) and (5) are equivalent to the well-known HNC integral equation [21]. The observations of Figs. 15–17 suggest that the basis for this theory should be revisited in the case of opposite sign charges with strong short distance coupling.

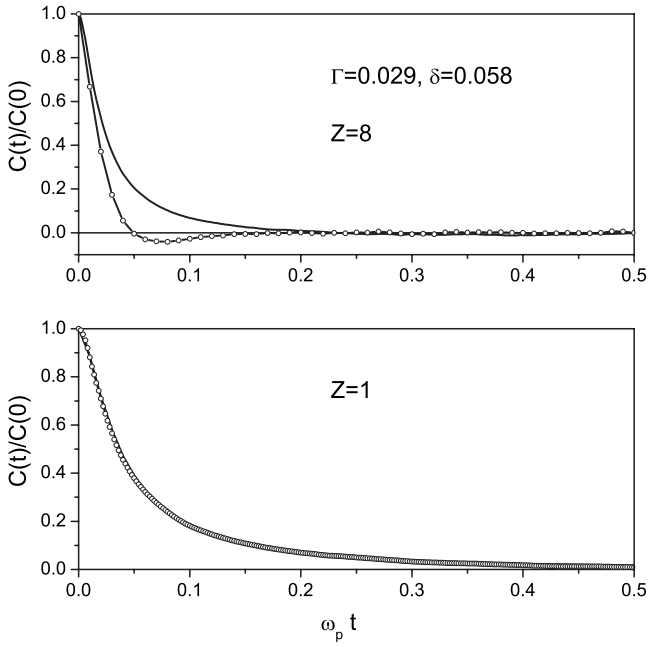

FIG. 15. Comparison of $C(t)$ from MD with results from mean field kinetic theory for $Z=1,8$.

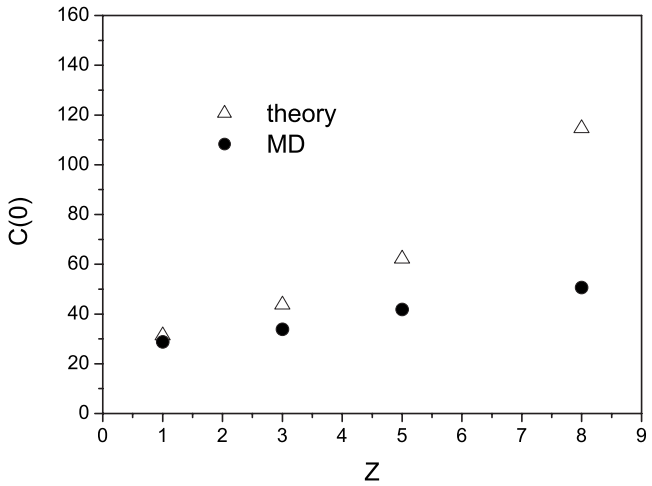

FIG. 16. Covariance as a function of Z at $\Gamma=0.029$.

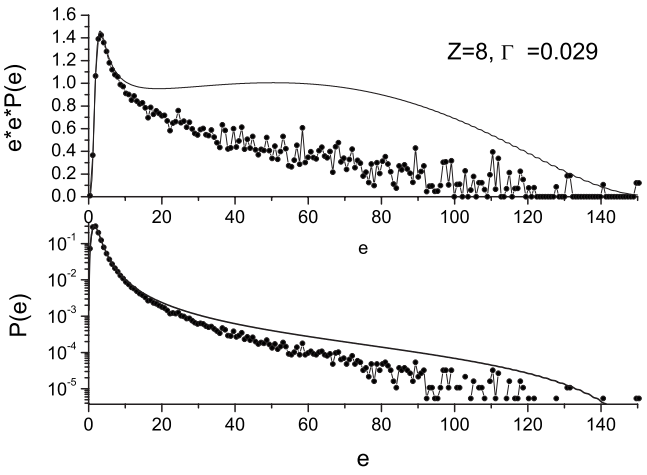

FIG. 17. Electric field distributions as a function of the field.

VII. SUMMARY

The objective here has been to explore the dynamics of electrons near a positive ion as a function of the charge number on the ion, or more precisely, as a function of the electron-ion coupling $\sigma = Z\Gamma/\delta$. A primary mathematical tool for this investigation has been molecular dynamics simulation, requiring a semiclassical regularization of the Coulomb potential at short distances. Under the hot, dense matter conditions needed to support large Z ions the electron coupling can be quite weak. An accurate theoretical description is then given by the nonlinear Vlasov kinetic equation for the electrons (with the qualifications of the last paragraph above). The MD simulation reveals an interesting structure for the electric field autocorrelation function. At the weakest electron-electron coupling considered there is a rapid initial decay followed by an asymptotic domain of weak anticorrelation. The time scale for the initial decay decreases with increasing Z but does not depend strongly on Z as long as the electron-ion coupling stays weak. This is illustrated in Fig. 7. Figures 5 and 6 show a quite different behavior at strong electron-ion coupling where the initial decay time shortens and the anticorrelation becomes prominent on the same time scale. This qualitative behavior is also characteristic of the single electron dynamics of the nearest neighbor. A quantitative description is provided by the Vlasov kinetic theory with the exact initial condition for the distribution of electrons about the ion, including strong electron-ion correlations mediated by weak electron-electron interactions. The mean field dynamics is that of effective single electron trajectories, calculated for the same effective potential as that for the initial correlations, and averaged over an ensemble of these initial states. The agreement between theory and simulation is generally quite reasonable. However, a discrepancy for the weakest electron-electron coupling (smallest δ) at large Z remains unresolved.

ACKNOWLEDGMENTS

Support for this research has been provided by the U.S. Department of Energy Grant No. DE-FG03-98DP00218. The authors thank M. Gigosos for helpful discussions and suggestions. J.D. is grateful for the support and hospitality of the University of Provence.

APPENDIX A: EVALUATION OF THE FIELD COVARIANCE

The dimensionless electric field covariance is defined by

$$C(0) = \frac{r_0^4}{e^2}\langle \mathbf{E}\cdot\mathbf{E}\rangle, \tag{A1}$$

with

$$\mathbf{E} = \sum_{\alpha=1}^{N_e} \mathbf{e}(\mathbf{r}_\alpha - \mathbf{r}_0). \tag{A2}$$

Here $\mathbf{r}_0$ denotes the position of the ion, chosen to be the origin in the following. The equilibrium average can be calculated directly in terms of the one and two electron charge densities

$$C(0) = \frac{r_0^4}{e^2}\int d\mathbf{r}\mathbf{e}(\mathbf{r})\cdot\left[n_e(r)\mathbf{e}(\mathbf{r}) + \int d\mathbf{r}' n_e(\mathbf{r},\mathbf{r}')\mathbf{e}(\mathbf{r}')\right], \tag{A3}$$

with the definitions

$$n_e(r_1) = N\frac{\int d\mathbf{r}_2\cdots d\mathbf{r}_N e^{-\beta U}}{\int d\mathbf{r}_1\cdots d\mathbf{r}_N e^{-\beta U}}, \tag{A4}$$

ne(r1,r2)=N(N−1)∫dr3···drNe−βU∫dr1···drNe−βU,where U is the total kinetic energy and $T = 1/k_B\beta$ is the temperature.

$$C(0) = -\frac{r_0^4}{Ze^3}\langle \nabla_{r_0} U_{ie}\cdot\mathbf{E}\rangle = \frac{r_0^4}{\beta Ze^3}\frac{\int d\mathbf{r}_1\cdots d\mathbf{r}_N(\nabla_{r_0}e^{-\beta U})\cdot\mathbf{E}}{\int d\mathbf{r}_1\cdots d\mathbf{r}_N e^{-\beta U}}$$

$$= \frac{r_0^4}{\beta Ze^3}\int d\mathbf{r}_1[\nabla_{r_0} n_e(|\mathbf{r}_1-\mathbf{r}_0|)]\cdot\mathbf{e}(\mathbf{r}_1-\mathbf{r}_0)$$

$$= -\frac{r_0^4}{\beta Ze^3}\int d\mathbf{r}[\nabla n_e(r)]\cdot\mathbf{e}(\mathbf{r}). \tag{A5}$$

Two forms of this last expression are useful in practice.

$$C(0) = \frac{r_0^4}{\beta Ze^3}\int d\mathbf{r}[n_e(r)-n_e]\nabla\cdot\mathbf{e}(\mathbf{r}), \tag{A6}$$

and

$$C(0) = \frac{r_0^4}{e^2}\int d\mathbf{r} n_e(r)\left(-\frac{1}{\beta Ze}\nabla\ \ln n_e(r)\right)\cdot\mathbf{e}(\mathbf{r})$$

$$= \frac{r_0^4}{e^2}\int d\mathbf{r} n_e(r)\mathbf{e}_{mf}(\mathbf{r})\cdot\mathbf{e}(\mathbf{r}). \tag{A7}$$

To obtain Eq. (A6) the boundary condition $n_e(\infty)=n_e$ has been used, and in the last equality of Eq. (A7) the mean force field has been introduced by

$$\mathbf{e}_{mf}(\mathbf{r}) = -\frac{1}{\beta Ze}\nabla \ln n_e(r). \tag{A8}$$

Finally, a comparison of Eqs. (A3) and (A7) gives the alternative expression for this field,

$$\mathbf{e}_{mf}(\mathbf{r}) = \mathbf{e}(\mathbf{r}) + \frac{1}{n_e(r)}\int d\mathbf{r}' n_e(\mathbf{r},\mathbf{r}')\mathbf{e}(\mathbf{r}'). \tag{A9}$$

APPENDIX B: KINETIC EQUATION FOR CORRELATION FUNCTIONS

In this Appendix the evaluation of the field autocorrelation function by kinetic theory, and the basis for the approximation (14), are briefly described. First, the correlation function is formally rewritten as

$$\begin{aligned} C(t) &= \frac{r_0^4}{e^2}\langle \mathbf{E}(t)\cdot\mathbf{E}\rangle = \frac{r_0^4}{e^2}\int d\mathbf{r}_1 d\mathbf{v}_1 \cdots d\mathbf{r}_N d\mathbf{v}_N \mathbf{E}\cdot\mathbf{E}(-t)\rho_e \\ &= \frac{r_0^4}{e^2}\int d\mathbf{r}_1 d\mathbf{v}_1 \mathbf{e}(\mathbf{r}_1) N \cdot \int d\mathbf{r}_2 d\mathbf{v}_2 \cdots d\mathbf{r}_N d\mathbf{v}_N \mathbf{E}(-t)\rho_e \\ &= \frac{r_0^4}{e^2}\int d\mathbf{r}_1 d\mathbf{v}_1 \mathbf{e}(\mathbf{r}_1)\cdot\psi(\mathbf{r}_1,\mathbf{v}_1;t), \end{aligned} \tag{B1}$$

where ρ_e is the equilibrium Gibbs ensemble and $\mathbf{e}(\mathbf{r}_\alpha)$ is the single particle field of Eq. (8). The integrations over degrees of freedom $2\cdots N$ in the second equality define a reduced function $\psi(\mathbf{r}_1,\mathbf{v}_1;t)$, which is the first member of a set of such functions

$$\psi^{(s)}(\mathbf{r}_1,\mathbf{v}_1;\cdots\mathbf{r}_s,\mathbf{v}_s;t) = N^s\int d\mathbf{r}_{s+1} d\mathbf{v}_{s+1}\cdots d\mathbf{r}_N d\mathbf{v}_N \mathbf{E}(-t)\rho_e. \tag{B2}$$

It is straightforward to verify that these functions satisfy the BBGKY hierarchy, whose first equation is formally the same as Eq. (11),

$$\begin{aligned} &(\partial_t + \mathbf{v}\cdot\nabla_{\mathbf{r}} - m_e^{-1}\{\nabla_{\mathbf{r}}[V_{ei}(\mathbf{r}) + V_{eb}(\mathbf{r})]\}\cdot\nabla_{\mathbf{v}})\psi(\mathbf{r}_1,\mathbf{v}_1;t) \\ &= m_e^{-1}\int d\mathbf{r}_2 d\mathbf{v}_2[\nabla_{\mathbf{r}} V_{ee}(\mathbf{r}-\mathbf{r}_2)]\cdot\nabla_{\mathbf{v}}\psi^{(2)}(\mathbf{r},\mathbf{v};\mathbf{r}_2,\mathbf{v}_2;t). \end{aligned} \tag{B3}$$

However, in contrast to the distribution functions in Eq. (11) the functional relationship of $\psi^{(2)}$ to ψ is linear. To see this, consider first the initial conditions which are found to be

$$\psi(\mathbf{r}_1,\mathbf{v}_1;t=0) = f_e(\mathbf{r}_1,\mathbf{v}_1)\mathbf{e}(\mathbf{r}_1) + \int d\mathbf{r}_2 d\mathbf{v}_2 f_e^{(2)} \times(\mathbf{r}_1,\mathbf{v}_1;\mathbf{r}_2,\mathbf{v}_2)\mathbf{e}(\mathbf{r}_2), \tag{B4}$$

or, equivalently,

$$\mathbf{e}(\mathbf{r}_1) = \frac{1}{f_e(\mathbf{r}_1,\mathbf{v}_1)}\left[\psi(\mathbf{r}_1,\mathbf{v}_1;t=0) - \int d\mathbf{r}_2 d\mathbf{v}_2 f_e^{(2)} \times(\mathbf{r}_1,\mathbf{v}_1;\mathbf{r}_2,\mathbf{v}_2)\mathbf{e}(\mathbf{r}_2)\right]. \tag{B5}$$

Next, this is substituted into the expression for $\psi^{(2)}(\mathbf{r}_1,\mathbf{v}_1;\mathbf{r}_2,\mathbf{v}_2;t=0)$,

$$\begin{aligned} \psi^{(2)}(\mathbf{r}_1,\mathbf{v}_1;\mathbf{r}_2,\mathbf{v}_2;t=0) &= f_e^{(2)}(\mathbf{r}_1,\mathbf{v}_1;\mathbf{r}_2,\mathbf{v}_2)[\mathbf{e}(\mathbf{r}_1)+\mathbf{e}(\mathbf{r}_2)] \\ &\quad + n\int d\mathbf{r}_3 d\mathbf{v}_3 f_e^{(3)}(\mathbf{r}_1,\mathbf{v}_1;\mathbf{r}_2,\mathbf{v}_2;\mathbf{r}_3,\mathbf{v}_3)\mathbf{e}(\mathbf{r}_3) \\ &= f_e^{(2)}(\mathbf{r}_1,\mathbf{v}_1;\mathbf{r}_2,\mathbf{v}_2)\left(\frac{\psi(\mathbf{r}_1,\mathbf{v}_1;0)}{f_e(\mathbf{r}_1,\mathbf{v}_1)} + \frac{\psi(\mathbf{r}_2,\mathbf{v}_2;0)}{f_e(\mathbf{r}_2,\mathbf{v}_2)}\right) + n\int d\mathbf{r}_3 d\mathbf{v}_3 h_e^{(3)} \\ &\quad \times(\mathbf{r}_1,\mathbf{v}_1;\mathbf{r}_2,\mathbf{v}_2;\mathbf{r}_3,\mathbf{v}_3)\mathbf{e}(\mathbf{r}_3). \end{aligned} \tag{B6}$$

Here, $f_e^{(s)}$ are the equilibrium s-particle reduced distribution functions associated with the Gibbs ensemble and $h_e^{(3)}$ is the equilibrium correlation function for three electrons in the presence of the ion

$$\begin{aligned} &h_e^{(3)}(\mathbf{r}_1,\mathbf{v}_1;\mathbf{r}_2,\mathbf{v}_2;\mathbf{r}_3,\mathbf{v}_3;t) \\ &= f_e^{(3)}(\mathbf{r}_1,\mathbf{v}_1;\mathbf{r}_2,\mathbf{v}_2;\mathbf{r}_3,\mathbf{v}_3) - f_e^{(2)}(\mathbf{r}_1,\mathbf{v}_1;\mathbf{r}_2,\mathbf{v}_2)\frac{1}{f_e(\mathbf{r}_1,\mathbf{v}_1)}f_e^{(2)} \\ &\times(\mathbf{r}_1,\mathbf{v}_1;\mathbf{r}_3,\mathbf{v}_3) - f_e^{(2)}(\mathbf{r}_1,\mathbf{v}_1;\mathbf{r}_2,\mathbf{v}_2)\frac{1}{f_e(\mathbf{r}_2,\mathbf{v}_2)}f_e^{(2)} \\ &\times(\mathbf{r}_2,\mathbf{v}_2;\mathbf{r}_3,\mathbf{v}_3). \end{aligned} \tag{B7}$$

The linear functional relationship between $\psi^{(2)}$ to ψ at $t=0$ is now evident.

$$\begin{aligned} \psi^{(2)}(\mathbf{r}_1,\mathbf{v}_1;\mathbf{r}_2,\mathbf{v}_2;0) &= f_e^{(2)}(\mathbf{r}_1,\mathbf{v}_1;\mathbf{r}_2,\mathbf{v}_2;t) \\ &\quad\times\left(\frac{\psi(\mathbf{r}_1,\mathbf{v}_1;0)}{f_e(\mathbf{r}_1,\mathbf{v}_1)} + \frac{\psi(\mathbf{r}_2,\mathbf{v}_2;0)}{f_e(\mathbf{r}_2,\mathbf{v}_2)}\right) \\ &\quad + 3 \text{ electron correlations.} \end{aligned} \tag{B8}$$

Recognizing this linear relationship, the basic approximation for weak coupling among the electrons is to neglect all of their correlations at all times, i.e., extend Eq. (B8) to

$$\begin{aligned} \psi^{(2)}(\mathbf{r}_1,\mathbf{v}_1;\mathbf{r}_2,\mathbf{v}_2;t) &\to f_e(\mathbf{r}_2,\mathbf{v}_2;t)\psi(\mathbf{r}_1,\mathbf{v}_1;t) \\ &\quad + f_e(\mathbf{r}_1,\mathbf{v}_1;t)\psi(\mathbf{r}_2,\mathbf{v}_2;t). \end{aligned} \tag{B9}$$

Use of this in the first hierarchy equation (B3) gives directly the kinetic equation (15) discussed in the text.

$$\begin{aligned} (\partial_t + \mathcal{L})\psi(\mathbf{r},\mathbf{v};t) &= -\beta f_e(\mathbf{r},\mathbf{v})\mathbf{v}\cdot\nabla_{\mathbf{r}}\int d\mathbf{r}_2 V_{ee} \\ &\quad\times(\mathbf{r}-\mathbf{r}_2)\int d\mathbf{v}_2\psi(\mathbf{r}_2,\mathbf{v}_2,t), \end{aligned} \tag{B10}$$

$$\mathcal{L} = \mathbf{v}\cdot\nabla_{\mathbf{r}} - m_e^{-1}[\nabla_{\mathbf{r}} U_{ei}(\mathbf{r})]\cdot\nabla_{\mathbf{v}}. \tag{B11}$$

APPENDIX C: SOLUTION TO KINETIC EQUATION

The operator $\mathcal{L}$ in Eq. (B3) is the generator for single electron dynamics in the effective potential due to the ion $U_{ei}(\mathbf{r})$. The solution to the equation can be obtained in terms of this single electron dynamics by direct integration

$$\psi(\mathbf{r},\mathbf{v};t) = e^{-\mathcal{L}t}\psi(\mathbf{r},\mathbf{v};0) - \int_0^t d\tau e^{-\mathcal{L}(t-\tau)} f_e(\mathbf{r},\mathbf{v})\beta\mathbf{v}\cdot\boldsymbol{\nabla}_{\mathbf{r}} \int d\mathbf{r}_2 V_{ee} \times(\mathbf{r}-\mathbf{r}_2)\mathbf{I}(\mathbf{r}_2,\tau), \tag{C1}$$

$$\mathbf{I}(\mathbf{r},t) = \int d\mathbf{v}\psi(\mathbf{r},\mathbf{v},t). \tag{C2}$$

The initial condition is given by Eq. (B4) which, according to Eq. (A9), can also be written as

$$\psi(\mathbf{r}_1,\mathbf{v}_1;t=0) = f_e(\mathbf{r}_1,\mathbf{v}_1)\mathbf{e}_{mf}(\mathbf{r}_1). \tag{C3}$$

An equation for $\mathbf{I}(\mathbf{r},t)$ follows from the substitution of Eq. (C1) into Eq. (C2).

$$\mathbf{I}(\mathbf{r};t) = \int d\mathbf{v}e^{-\mathcal{L}t} f_e(\mathbf{r},\mathbf{v})\mathbf{e}_{mf}(\mathbf{r}) - \int_0^t d\tau \int d\mathbf{v}e^{-\mathcal{L}(t-\tau)} f_e(\mathbf{r},\mathbf{v})\beta\mathbf{v}\cdot\boldsymbol{\nabla}_{\mathbf{r}} \int d\mathbf{r}_2 \times V_{ee}(\mathbf{r}-\mathbf{r}_2)\mathbf{I}(\mathbf{r}_2,\tau). \tag{C4}$$

This is an integral equation for $\mathbf{I}(\mathbf{r};t)$, which can be written

$$\int_0^t d\tau \int d\mathbf{r}_2 \epsilon(\mathbf{r},t;\mathbf{r}_2,\tau)\mathbf{I}(\mathbf{r}_2;\tau) = \int d\mathbf{v}e^{-\mathcal{L}t} f_e(\mathbf{r},\mathbf{v})\mathbf{e}_{mf}(\mathbf{r}). \tag{C5}$$

The dielectric function $\epsilon(\mathbf{r},t-\tau;\mathbf{r}_2)$ is defined by

$$\epsilon(\mathbf{r},t-\tau;\mathbf{r}') = \delta(t-\tau)\delta(\mathbf{r}-\mathbf{r}') + \int d\mathbf{r}''\pi(\mathbf{r},t-\tau;\mathbf{r}'')V_{ee}(\mathbf{r}''-\mathbf{r}'), \tag{C6}$$

where the polarization function is

$$\pi(\mathbf{r},t;\mathbf{r}') = \int d\mathbf{v}e^{-\mathcal{L}t} f_e(\mathbf{r},\mathbf{v})\beta\mathbf{v}\cdot\boldsymbol{\nabla}_{\mathbf{r}}\delta(\mathbf{r}-\mathbf{r}'). \tag{C7}$$

With these results the correlation function from Eq. (B1) becomes

$$\begin{aligned} C(t) &= \frac{r_0^4}{e^2}\int d\mathbf{r}d\mathbf{v}\mathbf{e}(\mathbf{r})\cdot\psi(\mathbf{r},\mathbf{v};t) = \frac{r_0^4}{e^2}\int d\mathbf{r}\mathbf{e}(\mathbf{r})\cdot\mathbf{I}(\mathbf{r};t) \\ &= \frac{r_0^4}{e^2}\int_0^t d\tau \int d\mathbf{r}\mathbf{e}(\mathbf{r})\cdot\int d\mathbf{r}_2\epsilon^{-1}(\mathbf{r},\tau;\mathbf{r}_2,)\int d\mathbf{v}e^{-\mathcal{L}(t-\tau)} \\ &\quad\times f_e(\mathbf{r}_2,\mathbf{v})\mathbf{e}_{mf}(\mathbf{r}_2) \\ &= \frac{r_0^4}{e^2}\int_0^t d\tau \int d\mathbf{r}d\mathbf{v}\mathbf{e}_s(\mathbf{r},\tau)\cdot e^{-\mathcal{L}(t-\tau)} f_e(\mathbf{r},\mathbf{v})\mathbf{e}_{mf}(\mathbf{r}). \end{aligned} \tag{C8}$$

In the last equality the screened field $\mathbf{e}_s(\mathbf{r},t)$ has been introduced.

$$\mathbf{e}_s(\mathbf{r},t) \equiv \int d\mathbf{r}'\mathbf{e}(\mathbf{r}')\epsilon^{-1}(\mathbf{r}',t;\mathbf{r}). \tag{C9}$$

Finally, using the stationarity of $f_e(\mathbf{r},\mathbf{v})$ under the dynamics generated by $\mathcal{L}$ gives

$$\begin{aligned} C(t) &= \frac{r_0^4}{e^2}\int_0^t d\tau \int d\mathbf{r}d\mathbf{v} f_e(\mathbf{r},\mathbf{v})\mathbf{e}_s(\mathbf{r},\tau)\cdot e^{-\mathcal{L}(t-\tau)}\mathbf{e}_{mf}(\mathbf{r}) \\ &\equiv \frac{r_0^4}{e^2}\int_0^t d\tau \int d\mathbf{r}d\mathbf{v} f_e(\mathbf{r},\mathbf{v})\mathbf{e}_s(\mathbf{r},\tau)\cdot\mathbf{e}_{mf}[\mathbf{r}(t-\tau)]. \end{aligned} \tag{C10}$$

This is the form used in the text [Eq. (18)].

[1] J. W. Dufty, in *Strongly Coupled Plasmas*, edited by H. de Witt and F. Rogers (NATO ASI Series, Plenum, NY, 1987), p. 493.

[2] J. W. Dufty and L. Zogaib, in Strongly Coupled Plasma Physics: Proceedings of the Yamada Conference XXIV on Strongly Coupled Plasma physics, edited by S. Ichimaru (Elsevier Pub. B. V., Amsterdam, 1990), p. 533; J. W. Dufty and L. Zogaib, Phys. Rev. A **44**, 2612 (1991); J. W. Dufty, in *Physics of Non-Ideal Plasmas-Selected Papers*, edited by W. Ebeling, A. Forster, and R. Radtke (Teubner-Texte, Stuttgart, 1992), Vol. 26, p. 215; J. W. Dufty and L. Zogaib, Phys. Rev. E **47**, 2958 (1993).

[3] A. Alastuey, J. L. Lebowitz, and D. Levesque, Phys. Rev. A **43**, 2673 (1991).

[4] M. Berkovsky, J. W. Dufty, A. Calisti, R. Stamm, and B. Talin, Phys. Rev. E **51**, 4917 (1995).

[5] D. B. Boercker, C. A. Iglesias, and J. W. Dufty, Phys. Rev. A **36**, 2254 (1987).

[6] M. A. Berkovsky, J. W. Dufty, A. Calisti, R. Stamm, and B. Talin, Phys. Rev. E **54**, 4087 (1996).

[7] B. Talin, A. Calisti, and J. Dufty, Phys. Rev. E **65**, 056406 (2002).

[8] B. Talin and J. W. Dufty, Contrib. Plasma Phys. **41**, 195 (2001); B. Talin, A. Calisti, and J. W. Dufty, *ibid.* **41**, 195 (2001).

[9] J. W. Dufty, I. Pogorelov, B. Talin, and A. Calisti, J. Phys. A **36**, 6057 (2003).

[10] H. B. Nersisyan, C. Toepffer, and G. Zwicknagel, Phys. Rev. E **72**, 036403 (2005).

[11] A. Filinov, M. Bonitz, and W. Ebeling, J. Phys. A **36**, 5957 (2003); A. V. Filinov, V. O. Golubnychiy, M. Bonitz, W. Ebeling, and J. W. Dufty, Phys. Rev. E **70**, 046411 (2004).

[12] T. Pschiwul and G. Zwicknagel, J. Phys. A **36**, 6251 (2003); Contrib. Plasma Phys. **41**, 271 (2001).

[13] G. Norman, A. Valuev, and I. Valuev, J. Phys. IV **10**, Pr5-255

(2000); W. Ebeling, G. Norman, A. Valuev, and I. Valuev, Contrib. Plasma Phys. **39**, 61 (1999); J. Ortner, I. Valuev, and W. Ebeling, *ibid.* **39**, 311 (1999).

[14] J. W. Dufty and M. Berkovsky, Nucl. Instrum. Methods Phys. Res. B **96**, 626 (1995).

[15] J. W. Dufty and M. Berkovsky, in *Physics of Strongly Coupled Plasmas*, edited by W. Kraeft, M. Schlanges, H. Haberland, and T. Bornath (World Scientific, River Edge, NJ, 1996).

[16] G. Zwicknagel, C. Toepffer, and P.-G. Reinhard, Phys. Rep. **309**, 118 (1999).

[17] R. Kubo, A Stochastic Theory of Line Shape and Relaxation, in *Fluctuation, Relaxation, and Resonance in Magnetic Systems*, edited by D. ter Haar (Oliver and Boyd, Edinburgh, 1962).

[18] B. Talin, E. Dufour, A. Calisti, M. A. Gigosos, M. A. González, T. del Río Gaztelurrutia, and J. W. Dufty, J. Phys. A **36**, 6049 (2003); E. Dufour, A. Calisti, B. Talin, M. Gigosos, M. A. González, and J. Dufty, J. Quant. Spectrosc. Radiat. Transf. **81**, 125 (2003).

[19] E. Dufour, A. Calisti, B. Talin, M. A. Gigosos, M. A. González, T. del Río Gaztelurrutia, and J. W. Dufty, Phys. Rev. E **71**, 066409 (2005).

[20] H. Minoo, M. M. Gombert, and C. Deutsch, Phys. Rev. A **23**, 924 (1981)

[21] J.-P. Hansen and I. MacDonald, *Theory of Simple Liquids* (Academic Press, San Diego, 1990).

[22] J. A. McLennan, *Introduction to Nonequilibrium Statistical Mechanics* (Prentice-Hall, Englewood, New Jersey, 1989).

[23] M. Lewis, Phys. Rev. **121**, 501 (1964); C. Cohen-Tannoudji, *Aux Frontières de la Spectroscopie Laser* (North-Holland Publishing Company, Amsterdam, 1975), Vol. 1.

[24] Th. Winkler *et al.*, Nucl. Instrum. Methods Phys. Res. A **391**, 12 (1997)

[25] H. Hegazy, S. Seidel, Th. Wrubel, and H.-J. Kunze, J. Quant. Spectrosc. Radiat. Transf. **81**, 221 (2003); Yu. V. Ralchenko, H. R. Griem, and I. Bray, *ibid.* **81**, 371 (2003).